# Enhanced Yield of Methyl Ethyl Ketone through Levulinic Acid Decarboxylation in the AgNO3/K2S2O8 System: Mechanistic Insights and Characterization of Metallic Species

Nydia Ileana Guzman Barrera, Jérôme Peydecastaing, Jérôme Esvan, Joël Albet, Carlos Vaca-Garcia, Philippe Behra, Emeline Vedrenne, Sophie Thiébaud-Roux

molecules

MDPI

*Article*

# Enhanced Yield of Methyl Ethyl Ketone through Levulinic Acid Decarboxylation in the $AgNO_3/K_2S_2O_8$ System: Mechanistic Insights and Characterization of Metallic Species

**Nydia I. Guzmán Barrera [1], Jérôme Peydecastaing [1], Jérôme Esvan [2], Joël Albet [1], Carlos Vaca-Garcia [1], Philippe Behra [1], Emeline Vedrenne [1] and Sophie Thiébaud-Roux [1,*]**

[1] Laboratoire de Chimie Agro-Industrielle (LCA), Université de Toulouse, INRAE, Toulouse INP, 31030 Toulouse, France; nydiaiguzman@gmail.com (N.I.G.B.); jerome.peydecastaing@toulouse-inp.fr (J.P.); joel.albet@toulouse-inp.fr (J.A.); carlos.vacagarcia@toulouse-inp.fr (C.V.-G.); philippe.behra@toulouse-inp.fr (P.B.); emeline.vedrenne@ensiacet.fr (E.V.)

[2] CIRIMAT, Université de Toulouse, Toulouse INP, CNRS, 31030 Toulouse, France; jerome.esvan@ensiacet.fr

* Correspondence: sophie.thiebaudroux@ensiacet.fr; Tel.: +33-5-3432-3500

**Abstract:** Methyl ethyl ketone (MEK) is among the most extensively utilized solvents in various industrial applications. In this study, we present a highly efficient synthesis route for MEK via the decarboxylation of biomass-derived levulinic acid, using potassium persulfate ($K_2S_2O_8$) and silver nitrate ($AgNO_3$) as key reagents. The specific roles of $AgNO_3$ and $K_2S_2O_8$ were thoroughly investigated. Additional silver species, such as $Ag_2O$ and AgO, were also detected during the reaction. X-ray photoelectron spectroscopy (XPS) and X-ray diffraction (XRD) analyses provided evidence of the evolution of solid phases throughout the reaction. Based on these findings, we propose a radical decarboxylation mechanism initiated by the generation of sulfate radicals ($SO_4\bullet-$) through the catalytic breakdown of $K_2S_2O_8$ by $AgNO_3$. This mechanistic understanding, combined with a parametric study, enabled us to achieve an unprecedented level of levulinic acid conversion (97.9%) and MEK yield (86.6%) with this system, surpassing all previously reported results in the literature.

**Keywords:** decarboxylation mechanism; methyl ethyl ketone synthesis; thermodynamic calculations; solid intermediate characterization; levulinic acid reactivity



**Citation:** Guzmán Barrera, N.I.; Peydecastaing, J.; Esvan, J.; Albet, J.; Vaca-Garcia, C.; Behra, P.; Vedrenne, E.; Thiébaud-Roux, S. Enhanced Yield of Methyl Ethyl Ketone through Levulinic Acid Decarboxylation in the $AgNO_3/K_2S_2O_8$ System: Mechanistic Insights and Characterization of Metallic Species. *Molecules* **2024**, *29*, 4822. https://doi.org/10.3390/molecules29204822

Academic Editors: Rosa Iacovino and Gianluca D'Abrosca

Received: 15 July 2024
Revised: 3 October 2024
Accepted: 4 October 2024
Published: 11 October 2024



## 1. Introduction

Methyl ethyl ketone (MEK) is widely utilized in the paint and surface coating industries, primarily as a low-boiling-point solvent for nitrocellulose, acrylic, and vinyl compounds. It is also frequently employed in professional paint shops and by painters for thinning acrylics and lacquers [1,2].

In the context of a growing bioeconomy, the use of biomass feedstocks has become increasingly attractive as a means to reduce carbon footprints and decrease reliance on fossil resources. Therefore, research into the synthesis of MEK from renewable raw materials, such as levulinic acid (LA), is particularly relevant, especially when utilizing environmentally sustainable processes.

Levulinic acid has been identified by the National Renewable Energy Laboratory (NREL) as one of the most valuable chemicals that can be produced from sugars or lignocellulosic biomass through acid dehydration [3]. It is an abundant chemical building block, with reported demand reaching 2606.2 tons in 2013 [4]. LA serves as a precursor to a wide range of valuable compounds, including tetrahydrofuran (THF), 2-methyltetrahydrofuran (2-MeTHF), levulinate esters, γ-valerolactone (GVL), α-angelica lactone, 1,4-pentanediol (PDO), acrylic acid, β-acetyl acrylic acid, and α-aminolevulinic acid [3,5].

The decarboxylation of heteroaromatic carboxylic acids [6–9], particularly with the use of high temperatures and Brønsted-Lewis acid catalysts such as $SiO_2$-$Al_2O_3$ and γ-

$Al_2O_3$ [10], has been extensively studied, whereas the decarboxylation of aliphatic carboxylic acids like LA remains less explored. Hydroxyl radicals (•OH) have been reported in the decarboxylation of aliphatic organic acids, such as 2-methylalanine and amino acids [11–15]. Furthermore, metal oxidants including Pb(IV), Co(III), Mn(III), Fe(II), Cu(II), and Ag (I) have also been examined [16–21].

Only a few studies have specifically addressed the decarboxylation of LA. Chum et al. reported the photoelectrochemical decarboxylation of LA using n-$TiO_2$ as a semiconductor, but the MEK yield was very low (0.0025–0.01%) [22]. In addition to MEK, products such as methanol, ethanol, propionic acid, acetic acid, acetone, acetaldehyde, ethyl acetate, methane, and ethane were also observed. More recently, Gong et al. described LA decarboxylation using cupric oxide as a catalyst under harsh conditions (300 °C), achieving a MEK yield of 67.5%, alongside acetone and acetic acid production [23]. Gong et al. also investigated LA decarboxylation using $AgNO_3/K_2S_2O_8$ as co-reagents at 160 °C for 30 min in an aqueous $NaOH/KH_2PO_4$ solution at pH 5, obtaining a moderate MEK yield of 44.2% under these milder conditions [24]. Mehrer et al. explored the decarboxylation of LA using an engineered *E. coli* strain, yielding 76% MEK [25]. Additionally, LA decarboxylation as a side reaction during LA hydrodeoxygenation with sulfided $NiMo/Al_2O_3$ catalyst was reported by Grilc and Likozar [26], while low yields of MEK (6%) were observed during LA hydroconversion with $Ni/SiO_2$ as a catalyst [27].

Decarboxylation reactions involving the $Ag(I)/K_2S_2O_8$ system have garnered significant interest from researchers [28–34]. It has been proposed that the decarboxylation mechanism in this system involves the oxidation of Ag(I) to Ag(II) by $S_2O_8^{2-}$, with Ag(II) subsequently promoting the formation of carboxyl radicals, leading to decarboxylation and the formation of the corresponding alkyl radicals [35].

The primary goal of this study was to optimize the decarboxylation of LA for MEK synthesis using the $AgNO_3/K_2S_2O_8$ system under milder conditions and to elucidate the reaction mechanism. We first investigated the speciation of silver and its interaction with $K_2S_2O_8$. Through the optimization of experimental conditions, we achieved an exceptional MEK yield of 86.6%. Finally, XPS and XRD analyses were performed to characterize the solid phases involved, providing strong support for the proposed reaction mechanism.

## 2. Results and Discussion

The decarboxylation of levulinic acid (LA) was studied in an aqueous phosphate solution, following the methodology previously described by Gong et al. [23,24]. The experimental setup involved multiphase systems composed of solid Ag salts, an aqueous solution containing LA and $K_2S_2O_8$, and a gaseous phase corresponding to the vapor pressure of the reactants and products.

### *2.1. Influence of $K_2S_2O_8$ and $AgNO_3$*

To clarify the individual roles of $K_2S_2O_8$ and $AgNO_3$ in LA decarboxylation, reactions were conducted at 100 °C without one of these components. When silver nitrate was added alone, no LA decarboxylation was observed after 30 min of reaction (Table 1, entry #1). However, when $K_2S_2O_8$ was used without $AgNO_3$, the reaction proceeded to varying degrees depending on the conditions. Using 0.25 equivalents of $K_2S_2O_8$ yielded trace amounts of methyl ethyl ketone (MEK) (2.6%) and acetic acid (AcOH) (1%) (Table 1, entry, #2). Increasing the persulfate concentration raised LA conversion from 3.6% to 18.8% (Table 1, entries #2–#5). The thermal decomposition of persulfate to generate sulfate radicals ($SO_4$•–) in aqueous solutions, as previously reported [30,36–43], likely explains the decarboxylation observed without $AgNO_3$. However, at higher $K_2S_2O_8$ concentrations (1–2 equivalents), LA conversion increased while MEK yield decreased (to 4.3%), with a corresponding increase in acetic acid production (14.5%) (Table 1, entries #4 and #5).

**Table 1.** Influence of $AgNO_3$ and $K_2S_2O_8$ on LA decarboxylation.

| # | $n_{eq}$ * $AgNO_3/K_2S_2O_8$ | Initial pH | Final pH | LA Conversion (%) | AcOH Yield (%) | MEK Yield (%) |
|---|---|---|---|---|---|---|
| 1 | 1/0 | 5 | 4 | 0.0 | 0.0 | 0.0 |
| 2 | 0/0.25 | 5 | 5 | 3.6 | 1.0 | 2.6 |
| 3 | 0/0.5 | 5 | 5 | 12.1 | 3.3 | 8.8 |
| 4 | 0/1 | 4 | 2 | 13.6 | 6.8 | 6.8 |
| 5 | 0/2 | 4 | 1 | 18.8 | 14.5 | 4.3 |

* $n_{eq}$ = number of equivalents with respect to LA. Experimental conditions: $K_2HPO_4/KH_2PO_4$ (0.1/0.1 M), 100 °C, 30 min.

In the absence of $AgNO_3$, the decarboxylation of LA by thermal persulfate decomposition at low pH (pH < 3; 100 °C) can be explained by the mechanism described in Equations (1)–(4).

$$S_2O_8^{2-} \rightarrow 2\,SO_4^{-}\bullet \quad (1)$$

$$CH_3COCH_2CH_2COOH + SO_4^{-}\bullet \rightarrow CH_3COCH_2CH_2COO\bullet + HSO_4^{-} \quad (2)$$

$$CH_3COCH_2CH_2COO\bullet + H_2O \rightarrow CH_3COCH_2CH_3 + CO_2 + OH\bullet \quad (3)$$

$$2\,OH\bullet \rightarrow H_2O + \frac{1}{2}\,O_2 \quad (4)$$

The role of $K_2S_2O_8$ in MEK production was further examined by investigating the reaction kinetics with 1 equivalent of $K_2S_2O_8$ (Table 1). The MEK yield was highest in the early stages of the reaction but began to decline as acetic acid production increased (Figure 1). This behavior was explored by subjecting MEK to the same reaction conditions in the presence of potassium persulfate. A 10% conversion of MEK into acetic acid was observed after 30 min at 100 °C (see Section 2.3, Scheme 2). These results indicate that during LA decarboxylation, MEK is partially oxidized to acetic acid, explaining the drop in MEK yield and the rise in acetic acid after 20 min of reaction. At 25 °C, MEK was also converted to acetic acid but in smaller amounts, suggesting that temperature plays a crucial role in MEK oxidation to AcOH.

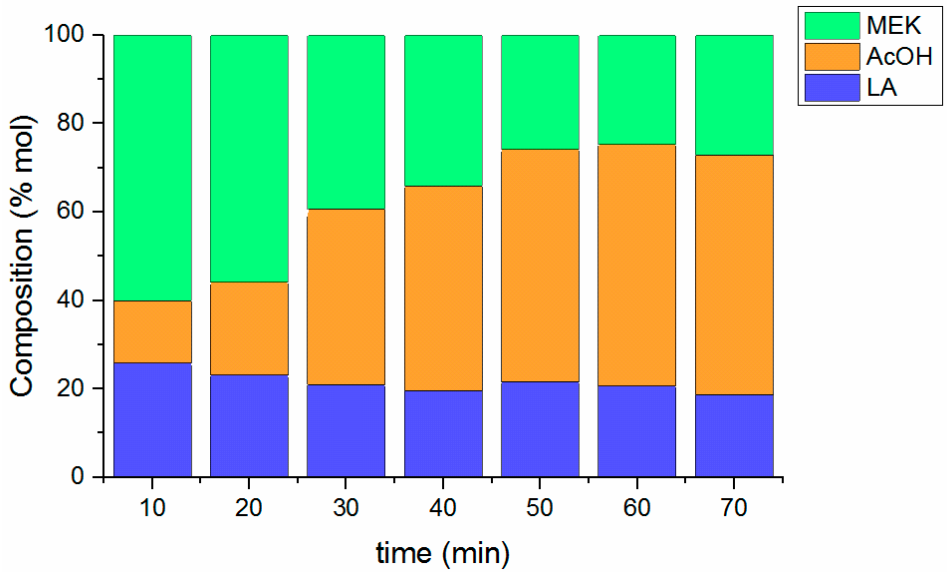


**Figure 1.** Decarboxylation of LA with 1 eq. of $K_2S_2O_8$ in the absence of $AgNO_3$. Experimental conditions: $K_2HPO_4/KH_2PO_4$ (0.1/0.1 M), 100 °C.

### 2.2. Role of Ag Salts

The decomposition of $K_2S_2O_8$ is known to be catalyzed by transition metals, including silver species [17,35,44]. To investigate the influence of different silver salts on LA decarboxylation, reactions were performed using a 1:1 ratio of Ag salt to $K_2S_2O_8$ at 100 °C. The presence of $AgNO_3$ significantly enhanced LA conversion (from 14% to 46.8%) and MEK yield (from 6.8% to 32%) (Table 1, entry #4 vs. Table 2, entry #1). With AgCl, MEK yield was slightly lower (25.2%) (Table 2, entry #2). In contrast, when $Ag_2O$ or AgO was used with persulfate, MEK yields were comparable to $AgNO_3$, but acetic acid production increased substantially (Table 2, entries #3 and #4). These results suggest that silver species catalyze $K_2S_2O_8$ decomposition, enhancing LA decarboxylation.

**Table 2.** Effect of different Ag salts on LA decarboxylation.

| # | Ag Salt | $n_{eq}$ Ag Salt/$K_2S_2O_8$ | Initial pH | Final pH | LA Conversion (%) | AcOH Yield (%) | MEK Yield (%) |
|---|---|---|---|---|---|---|---|
| 1 | $AgNO_3$ | 1/1 | 5 | 2 | 46.9 | 14.4 | 32.5 |
| 2 | AgCl | 1/1 | 6 | 5 | 38.7 | 13.5 | 25.2 |
| 3 | $Ag_2O$ | 1/1 | 4 | 3 | 54.3 | 17.8 | 36.5 |
| 4 | AgO | 1/1 | 5 | 3 | 57.6 | 22.9 | 34.8 |
| 5 | AgO | 1/0 | 4 | 1 | 0.0 | 0.0 | 0.0 |

Experimental conditions: $K_2HPO_4/KH_2PO_4$ (0.1/0.1 M), 100 °C, 30 min. Entry #1 is used for comparison in the following tables.

The decarboxylation mechanism involving Ag(I) and $K_2S_2O_8$, first proposed by Anderson and Kochi in 1970 [35] and later by other authors [24,32,45,46], suggests a catalytic cycle in which Ag(I) is oxidized to Ag(II) by persulfate or sulfate radicals. Ag(II) then promotes decarboxylation, regenerating Ag(I). A reaction with 1 equivalent of AgO (Ag(II)) without $K_2S_2O_8$ resulted in no LA conversion (Table 2, entry #5), confirming that $K_2S_2O_8$ is essential for LA decarboxylation. This points to a radical mechanism initiated by sulfate radicals ($SO_4\bullet-$) from $K_2S_2O_8$ decomposition. Our results are consistent with those reported by Seipled et al., who found that no arylation of various heterocycles occurred with arylboronic acid in the presence of Ag(II) as the sole oxidant [31].

### 2.3. Role of $K_2S_2O_8$ in the Presence of $AgNO_3$

To verify that levulinic acid (LA) decarboxylation proceeds via a radical mechanism, initiated by the decomposition of $K_2S_2O_8$ into sulfate radicals ($SO_4\bullet-$), a reaction was performed with the radical scavenger TEMPO ((2,2,6,6-tetramethylpiperidin-1-yl)oxyl). The reaction conditions were the same as those used for $AgNO_3/K_2S_2O_8$ (1/1 equivalent) with the addition of 1 or 2 equivalents of TEMPO. The complete suppression of LA conversion confirmed the radical nature of the reaction, specifically that the persulfate ions break down into $SO_4\bullet-$, which are responsible for LA decarboxylation [Reaction (a), Scheme 1]. Additionally, the pH of the solution decreased during the reaction, attributed to the formation of bisulfate ions ($HSO_4^-$), a weak acid ($pKa_2$ = 1.9 at 25 °C and 2.98 at 99 °C) [Equation (5)].

$$H_2SO_4^- + H_2O \leftrightarrow H_3O^+ + HSO_4^{2-} \quad (5)$$

Under such acidic conditions, $S_2O_8^{2-}$ can further decompose into sulfuric acid and Caro's acid ($H_2SO_5$), [Reaction (b), Scheme 2] [37], contributing to the observed pH decrease. The formation of hydrogen peroxide ($H_2O_2$) [Reaction (c)] and its subsequent reduction to oxygen ($O_2$) leads to the regeneration of Ag(I) [Reaction (d), Scheme 2]. Additionally, a reaction between levulinic acid and Ag(II) may occur [Reaction (a'), Scheme 2], producing the same radical intermediates along with Ag(I) and $H^+$, which further decreases the solution pH.

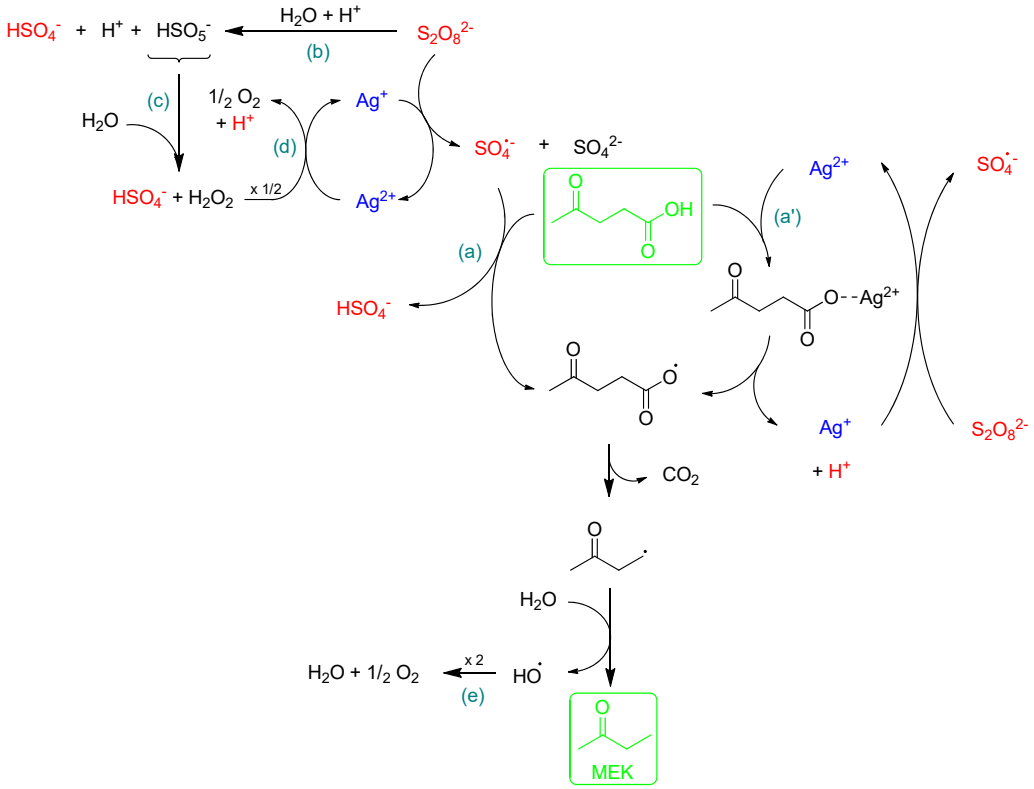


**Scheme 1.** Proposed mechanisms.

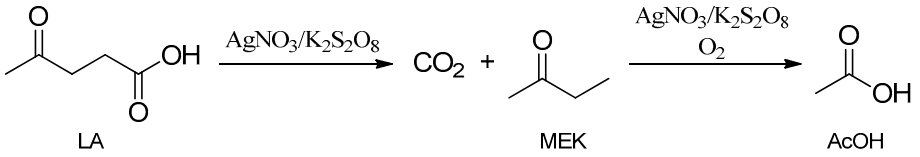


**Scheme 2.** AcOH production via MEK oxidation.

Given that the $AgNO_3/K_2S_2O_8$ system provided the highest MEK yields and the lowest acetic acid (AcOH) production (Table 2, entry #1), this combination was selected for further parametric study to gain deeper insight into the reaction mechanism.

### *2.4. Influence of $AgNO_3/K_2S_2O_8$ Ratio*

A series of reactions were conducted with varying $AgNO_3/K_2S_2O_8$ ratios. Lower LA conversions and MEK yields were observed with smaller amounts of $AgNO_3$ and $K_2S_2O_8$ (Table 3, entries #1 and #2). As observed in the absence of $AgNO_3$ (Table 1, entry #5), increasing the amount of $K_2S_2O_8$ to 2 equivalents led to increased AcOH production but did not enhance the MEK yield (Table 3, entry #4).

**Table 3.** Effect of $AgNO_3/K_2S_2O_8$ ratio on LA decarboxylation.

| # | $n_{eq}$ $AgNO_3/K_2S_2O_8$ | Initial pH | Final pH | LA Conversion (%) | AcOH Yield (%) | MEK Yield (%) |
|---|---|---|---|---|---|---|
| 1 | 0.5/0.5 | 5 | 3 | 22.8 | 13.6 | 9.2 |
| 2 | 1/0.5 | 5 | 2 | 34.2 | 15.8 | 18.4 |
| 3 | 1/1 | 5 | 2 | 46.9 | 14.4 | 32.5 |
| 4 | 1/2 | 4 | 1 | 49.2 | 21.3 | 27.9 |

Experimental conditions: $K_2HPO_4/KH_2PO_4$ (0.1/0.1 M), 100 °C, 30 min.

To confirm whether acetic acid forms as a result of MEK oxidation, a reaction was performed using MEK as the starting material in the presence of 1 equivalent each of $AgNO_3$ and $K_2S_2O_8$ at 100 °C. MEK conversion into AcOH was observed to be 10% and 17% after 30 and 60 min, respectively. This supports the hypothesis that during LA decarboxylation under acidic conditions, MEK can undergo subsequent oxidation to AcOH (Scheme 2). These findings align with those of Hobbs et al. [47], who demonstrated that MEK is oxidized to AcOH in the presence of $O_2$ and a metal catalyst. In this system, $O_2$ is generated during the reduction of Ag(II) to Ag(I) [Reaction (d), Scheme 1] and the termination reaction [Reaction (e), Scheme 1].

### *2.5. Influence of Temperature and Reaction Time*

A kinetic study of LA decarboxylation was conducted at 100 °C, 60 °C, and 25 °C to further understand and optimize MEK production (Figure 2). Reactions were carried out with 1 equivalent each of $AgNO_3$ and $K_2S_2O_8$. At 100 °C, MEK formation was faster than AcOH production, reaching a maximum yield after 5 min. At 60 °C, slightly more AcOH was produced, reaching 20% yield after 20 min, while MEK production was slower. At room temperature, more AcOH was produced than MEK (Figure 2c), suggesting that MEK oxidation to AcOH outpaces its production at lower temperatures.

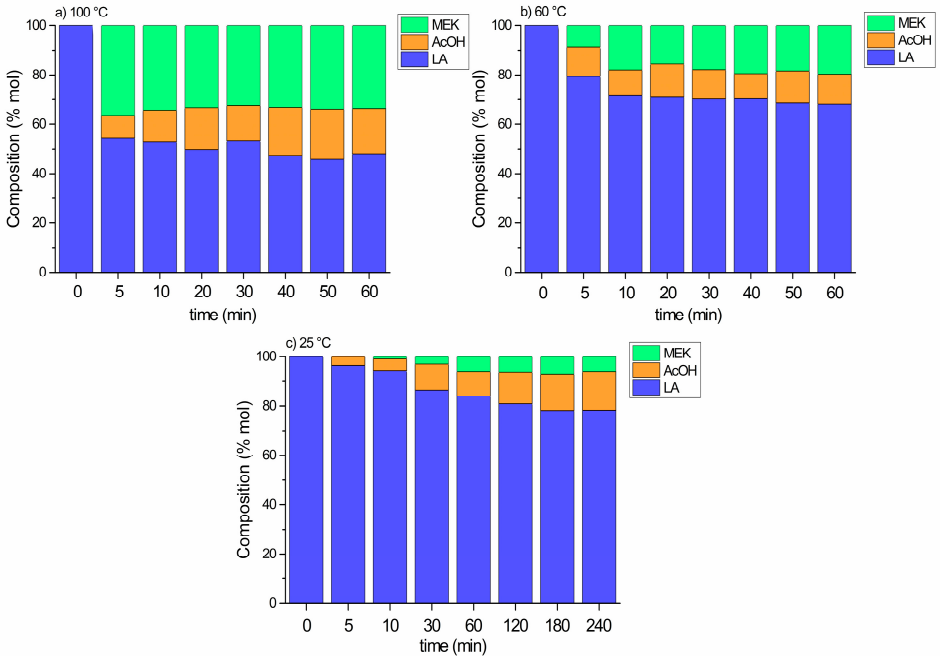


**Figure 2.** LA decarboxylation at different temperatures and reaction times (**a**) 100, (**b**) 60, and (**c**) 25 °C. Experimental conditions: $AgNO_3/K_2S_2O_8$ (1/1), $KH_2PO_4/K_2HPO_4$ (0.1/0.1 M).

Two phenomena may explain these observations: (i) at lower temperatures, $O_2$ is more soluble in the aqueous medium, promoting MEK oxidation [47]; and (ii) at higher temperatures, such as 100 °C, some of the MEK may be in the gaseous phase. However, ProSim® simulations of vapor–liquid equilibrium at 100 °C and atmospheric pressure indicated that less than 1% of MEK was in the gas phase, ruling out the second hypothesis. Therefore, MEK oxidation to AcOH appears to be linked to increased oxygen solubility at lower temperatures, while the increase in MEK production with temperature suggests that LA decarboxylation is an endothermic reaction, with the equilibrium shifting to favor MEK production at higher temperatures (Figure 2a). Similar behavior has been observed in the decarboxylation of malonic acid, butylmalonic acid, and 2-aminoisobutyric acid, where the reactions were also endothermic, with enthalpy changes (ΔH) ranging from 17.0 to 39.9 kcal/mol [48–50].

Given that low temperatures did not yield optimal results, reactions were conducted under identical conditions at 125 °C and 150 °C. However, no significant increase in MEK production was observed beyond 100 °C, with yields of 25% and 28% MEK at 125 °C and 150 °C, respectively.

### 2.6. Characterization of Solid Phases

X-ray diffraction (XRD) and X-ray photoelectron spectroscopy (XPS) were employed to examine the evolution of solid phases during the reaction, aiming to understand why MEK yields did not exceed 33%. A notable color change, from colorless to yellow, was observed upon the addition of $AgNO_3$ to a solution of phosphates ($KH_2PO_4/K_2HPO_4$) containing levulinic acid (LA) and potassium persulfate ($K_2S_2O_8$) at the start of the reaction, suggesting the formation of $Ag_3PO_4$. XRD analysis confirmed this, showing that the solid phases primarily consisted of $Ag_3PO_4$ with distinct diffraction peaks at 20.9°, 29.7°, 33.3°, 36.6°, 42.5°, 47.8°, 52.7°, 55.0°, 57.3°, 61.7°, 65.9°, 69.9°, and 71.9° (JCPDS No. 06-0505) [51]. Additionally, traces of $K_2S_2O_8$ (major peaks at 24.0, 25.9, 27.3, 27.6, 29.3, 32.7, 35.2, and 36.4°; ICSD No. 16972) [52], $Ag_2SO_4$ (major peaks at 22.2, 31.1, 33.8, 37.2, 47.0, and 53.5°) [53], $KH_2PO_4$ (major peaks at 23.8, 30.7, and 46.5°; ICSD 201371) [54], and $Ag_4P_2O_7$ (major peaks at 27.1, 32.3, and 32.5°) were also identified (Figure 3a).

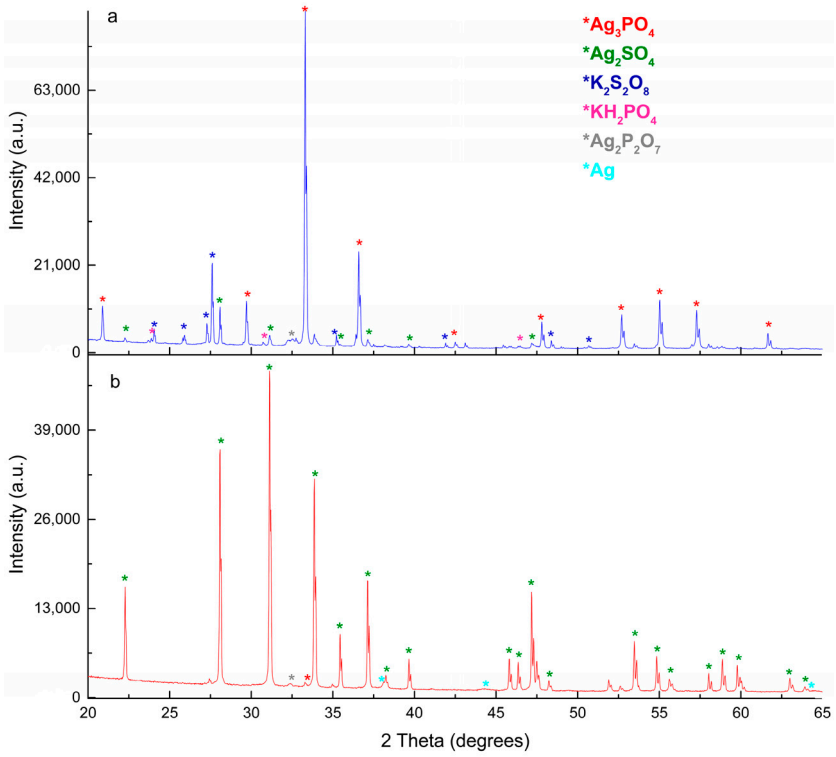


**Figure 3.** XRD patterns for the solid phase (**a**) before and (**b**) after the reaction. Experimental conditions: $AgNO_3/K_2S_2O_8$ (1/1), $KH_2PO_4/K_2HPO_4$ (0.2 M), 100 °C, 30 min.

$Ag_3PO_4$ likely forms from the reaction between $AgNO_3$ and $H_2PO_4^-/HPO_4^{2-}$, as represented by Equations (6) and (7).

$$3\,AgNO_3(s) + H_2PO_4^- \leftrightarrow Ag_3PO_4(s) + 3\,NO_3^- + 2\,H^+ \quad (6)$$

$$3\,AgNO_3(s) + HPO_4^{2-} \leftrightarrow Ag_3PO_4(s) + 3\,NO_3^- + H^+ \quad (7)$$

Subsequently, $Ag_4P_2O_7$ may be produced according to Equations (8) and (9).

$$2\,K_2HPO_4(s) \leftrightarrow K_4P_2O_7(s) + H_2O \quad (8)$$

$$4\ AgNO_3(s) + K_4P_2O_7(s) \leftrightarrow Ag_4P_2O_7(s) + 4\ NO_3^- + 4K^+ \quad (9)$$

Finally, $Ag_2SO_4$ can form via the interaction of $HSO_4^-$ with $AgNO_3$ (Equation (10)), with $HSO_4^-$ potentially generated by the decomposition of $K_2S_2O_8$ in aqueous medium at low pH, initiated by $AgNO_3$ or light (Equation (11)) [55–58].

$$2\ K_2S_2O_8(s) + 2\ H_2O \leftrightarrow 4\ HSO_4^- + 4\ K^+ + O_2(g) \quad (10)$$

$$HSO_4^- + 2\ AgNO_3(s) \leftrightarrow Ag_2SO_4(s) + 2\ NO_3^- + H^+ \quad (11)$$

XRD patterns obtained at the end of the reaction (Figure 3b) revealed that the solid phases predominantly contained $Ag_2SO_4$, with traces of $Ag_3PO_4$, $Ag_4P_2O_7$, $Ag_3O_4$, and elemental silver ($Ag^0$). This suggests that $Ag_3PO_4$ was converted into $Ag_2SO_4$ during the reaction. The formation of $Ag_2SO_4$ likely occurred via the reaction between $HSO_4^-$ and silver phosphate, as indicated by Equation (12).

$$2\ Ag_3PO_4(s) + 3\ HSO_4^- + 3\ H^+ \leftrightarrow 3\ Ag_2SO_4(s) + 2\ H_3PO_4 \quad (12)$$

Additionally, diffraction peaks for $Ag^0$ were observed at 38.6° (111), 44.3° (200), 64.4° (220), and 77.3° (311) [59], implying that elemental silver may form during the reaction. Previous studies by Deb et al. using XPS analysis showed $Ag^0$ formation during the oxidative trifluoromethylation of alkenes with $AgNO_3/K_2S_2O_8$, suggesting a catalytic cycle involving Ag(I)-Ag(0) [60]. Hatamura et al. also reported the reduction of Ag(I) to Ag(0) during the decarboxylation of Ag(I) β-ketocarboxylates [61].

XRD patterns revealed weak peaks at 27.7°, 33.5°, 35.8°, and 39.7° in the solid phase at the end of LA decarboxylation, which were attributed to $Ag_3O_4$ (ICSD No. 59225). However, the presence of $Ag_3O_4$ was deemed unlikely as this compound decomposes under X-ray irradiation at room temperature [62]. $Ag_3O_4$ is a binary oxide $Ag^{2+}(Ag^{3+})_2O_4$ [63], and its detection may be related to the presence of other oxide species.

XPS surface analyses were conducted to gain further insight into LA decarboxylation. The Ag $3d_{5/2}$ XPS spectrum at the beginning of the reaction showed a binding energy (BE) of 367.9 eV with a full width at half maximum (FWHM) of 1.17 eV (for Ag metal reference, FWHM < 0.8 eV), indicating a single silver oxidation state [64]. After the reaction, a slight shift to higher BE (368.05 eV) was observed, along with an increased FWHM of 1.46 eV, suggesting the presence of multiple silver species. The small BE shift made it difficult to determine the exact silver species involved, but Auger electron analysis revealed Ag oxide species. In the Auger spectra before and after the reaction (Figure 4), signals corresponding to $AgM_5N_{45}N_{45}$ and $AgM_4N_{45}N_{45}$ peaks were observed at 348.6 eV and 354.5 eV, which were attributed to $Ag_3PO_4$ [65]. A peak at 354.5 eV was also assigned to $Ag_2SO_4$ [66]. Furthermore, the presence of sulfates (S $2p_{3/2}$ at 169.24 eV) and phosphates (P $2p_{3/2}$ at 133.17 eV) was confirmed by XPS, corroborating the XRD results. After the reaction, additional Auger signals at 350.7 eV and 356.6 eV were attributed to $Ag_2O$ and AgO [67–69].

While $Ag_3O_4$ was identified in XRD patterns, neither $Ag_2O$ nor AgO were detected. These species may be present in amorphous forms on the solid surface, as indicated by XPS analyses. The mixed-valence nature of $Ag_3O_4$ ($Ag^{2+}(Ag^{3+})_2O_4$) may have interfered with the identification of $Ag_2O$ and AgO in XRD measurements.

Solid-phase analyses primarily revealed the presence of Ag(I) in various forms, such as $Ag_3PO_4$, $Ag_2SO_4$, and $Ag_4P_2O_7$, resulting from its interaction with the solution. Only trace amounts of Ag(II) and metallic Ag(0) were detected. The persistence of Ag(I) species throughout the reaction does not fully account for the observed limitations in LA decarboxylation. This may be attributed to the acidification of the reaction medium, which likely inhibits the generation of sulfate radicals ($SO_4\bullet-$) and instead promotes the formation of Caro's acid, a competing reaction pathway [Scheme 1, Reaction (b) vs. Reaction (a)].

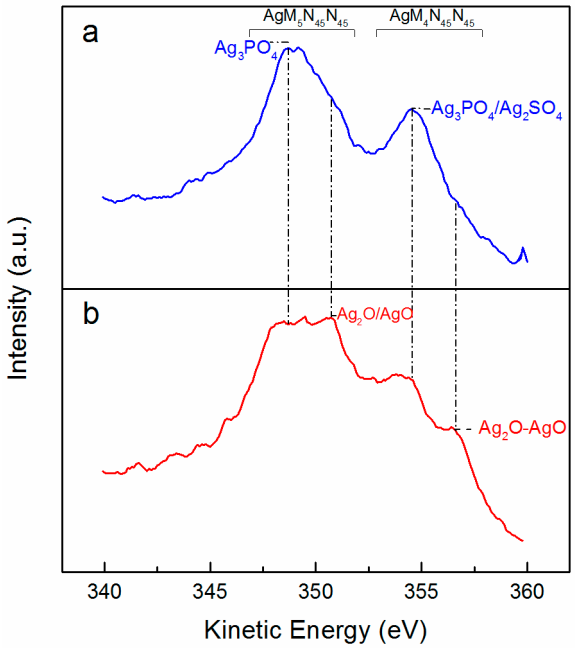


**Figure 4.** AgMNN Auger signals of the solid phase (**a**) before and (**b**) after levulinic acid decarboxylation.

### *2.7. Influence of pH Variation*

As described earlier, the pH of the reaction solution decreased during the reaction. The pH dropped from 5 to 2 or 1 as the concentration of $K_2S_2O_8$ increased, with neither the $K_2HPO_4/KH_2PO_4$ buffer solution nor other tested acid-base pairs able to stabilize the pH. A drop in LA conversion and MEK yield was observed when NaOH was used as the base (Table 4, entries #1 and #8). However, similar conversion rates and yields were obtained with $K_2HPO_4/KH_2PO_4$ and $KH_2PO_4$ solutions (Table 4, entries #2–#4 and #6). MEK yields slightly improved with $K_2HPO_4$ and $Na_2HPO_4/NaH_2PO_4$ solutions (Table 4, entries #5 and #7).

**Table 4.** Effect on LA decarboxylation of aqueous composition and initial pH.

| # | Aqueous Composition | Solution Concentration [M] | Solution pH * | Initial pH | Final pH | LA Conversion (%) | AcOH Yield (%) | MEK Yield (%) |
|---|---|---|---|---|---|---|---|---|
| 1 | Water | - | 6 | 3 | 1 | 29.6 | 14.8 | 14.8 |
| 2 | KCl/NaOH | 0.2 | 12 | 4 | 1 | 48.8 | 12.3 | 36.5 |
| 3 | $K_2HPO_4/KH_2PO_4$ | 0.2 | 7 | 5 | 2 | 46.9 | 14.4 | 32.5 |
| 4 | $K_2HPO_4/KH_2PO_4$ | 0.2 | 8 | 5 | 2 | 47.6 | 15.7 | 31.0 |
| 5 | $Na_2HPO_4/NaH_2PO_4$ | 0.2 | 7 | 4 | 2 | 50.5 | 10.9 | 39.6 |
| 6 | $KH_2PO_4$ | 0.2 | 4 | 3 | 1 | 48.9 | 21.3 | 27.9 |
| 7 | $K_2HPO_4$ | 0.2 | 8 | 5 | 1 | 50.0 | 11.0 | 39.0 |
| 8 | NaOH | $9 \times 10^{-4}$ | 8 | 5 | 1 | 30.5 | 9.7 | 20.8 |

* Solution pH measured at 25 °C before the addition of reactants. Experimental conditions: $AgNO_3/K_2S_2O_8$ (1/1), 100 °C, 30 min.

To counteract the decreasing pH, NaOH was added to adjust the solution pH to 5 after 30 min of reaction. When the reaction was allowed to proceed for an additional 30 min under these conditions, there was no further increase in LA conversion or MEK yield (Table 5, entries #1 and #2). However, when both NaOH and an additional equivalent of persulfate were introduced after 30 min, LA conversion increased significantly to 99%, and an excellent MEK yield of 87% was achieved, underscoring the importance of maintaining pH and persulfate concentration (Table 5, entry #3). These results indicate that the drop in pH during the reaction limits MEK production. When persulfate and silver nitrate were added without pH adjustment, a modest increase in MEK yield from 31% to 38% was

observed (Table 5, entry #5). However, in both cases, AcOH production increased. Thus, MEK production appears to be pH-dependent.

**Table 5.** Improvement of LA conversion and MEK yield following the adjustment of reaction pH.

| # | Description of Reaction | $n_{eq}$ $AgNO_3$/$K_2S_2O_8$ | Initial pH | Final pH | LA Conversion (%) | AcOH Yield (%) | MEK Yield (%) |
|---|---|---|---|---|---|---|---|
| 1 | Initial reaction: medium 1 (M1) [a] | 1/1 | 5 | 2 | 46.9 | 14.4 | 32.5 |
| | **After adjustment at pH 5** | | | | | | |
| 2 | Addition of NaOH to M1 [b] | 0/0 | 5 | 2 | 43.8 | 11.8 | 32.0 |
| 3 | Addition of NaOH/$K_2S_2O_8$ to M1 [b] | 0/1 | 5 | 1 | 97.9 | 11.3 | 86.6 |
| | **Without adjustment of pH** | | | | | | |
| 4 | Addition of $K_2S_2O_8$ to M1 [b] | 0/1 | 2 | 1 | 54.3 | 22.8 | 31.5 |
| 5 | Addition of $AgNO_3$/$K_2S_2O8$ to M1 [b] | 1/1 | 2 | 1 | 67.0 | 28.7 | 38.3 |

Experimental conditions: $AgNO_3$/$K_2S_2O_8$ (1/1), $KH_2PO_4$/$K_2HPO_4$ (0.1/0.1 M), 100 °C. [a] The first cycle of 30 min, [b] after the second cycle of 30 min.

XRD and XPS analyses of the solid phase were conducted following the addition of NaOH to the reaction medium and after the second reaction cycle to investigate the underlying causes for the observed increase in levulinic acid (LA) conversion and corresponding enhancement in MEK production after pH adjustment.

XRD patterns revealed that after pH adjustment with NaOH, the primary crystalline phase present was $Ag_3PO_4$, with minor amounts of $Ag_4P_2O_7$ and metallic silver ($Ag^0$) also detected (Figure 5a). The solid phase composition of the adjusted medium closely resembled that observed in the XRD patterns at the start of the first reaction cycle (Figure 3a). These findings suggest that the reaction medium can be regenerated by NaOH addition, which accounts for the improved LA conversion in the second reaction cycle.

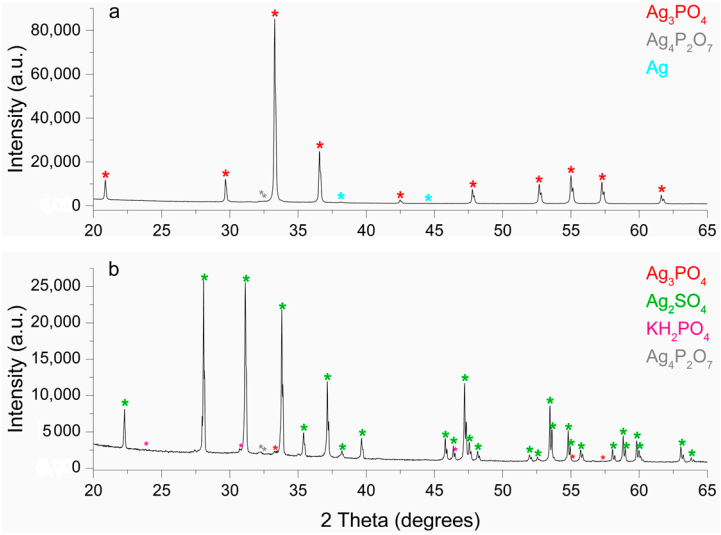


**Figure 5.** XRD patterns for the solid phase: (**a**) after M1 neutralization, (**b**) after the second cycle of the reaction, with the addition of $K_2S_2O_8$. Experimental conditions: $AgNO_3$/$K_2S_2O_8$ (1/1), $KH_2PO_4$/$K_2HPO_4$ (0.1/0.1 M), 100 °C.

The XRD patterns following the second reaction cycle are shown in Figure 5b. The conversion of $Ag_3PO_4$ to $Ag_2SO_4$ was observed, consistent with the results from the first reaction cycle (Figure 3b). $Ag_2SO_4$ was the dominant species present, along with residual traces of $Ag_3PO_4$, $KH_2PO_4$, and $Ag_4P_2O_7$.

The XPS analyses were in full agreement with the XRD results. In the Auger spectrum obtained following the addition of NaOH (Figure 6a), the peaks corresponding to the $Ag_2O$-AgO mixture, observed at kinetic energies of 350.7 eV (Ag $M_5N_{45}N_{45}$) and 356.6 eV (Ag

$M_4N_{45}N_{45}$) in Figure 4a, disappeared. This confirms that the medium can be regenerated by the addition of NaOH. The spectrum exhibited a profile similar to that observed at the start of the first reaction cycle. The formation of silver oxide species was further confirmed after the second reaction cycle, with the characteristic Auger peaks reappearing at 350.6 and 356.5 eV (Figure 6b).

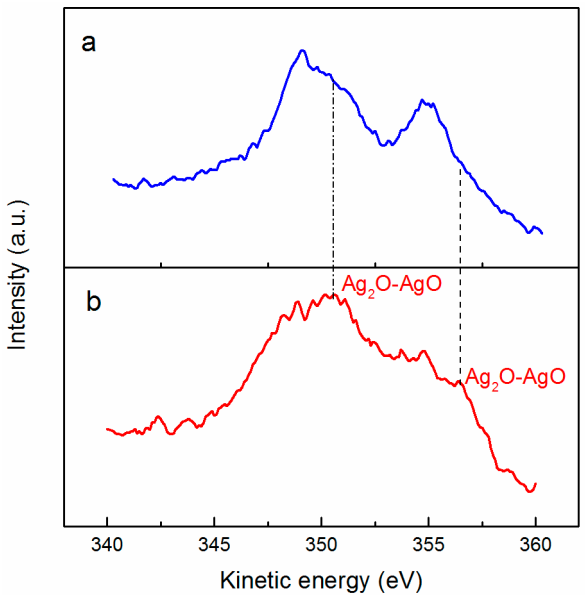


**Figure 6.** AgMNN Auger signals for the solid phase: (**a**) after M1 neutralization, (**b**) after the second cycle of reaction. Experimental conditions: $AgNO_3/K_2S_2O_8$ (1/1), $KH_2PO_4/K_2HPO_4$ (0.1/0.1 M), 100 °C, 30 min.

These findings suggest that $AgNO_3$ can be effectively reused in subsequent reactions, with only the replenishment of $K_2S_2O_8$ needed to maintain high levels of LA conversion and MEK yield. This study represents a significant advancement toward the development of more sustainable and environmentally friendly processes for MEK production.

## 3. Materials and Methods

### *3.1. LA Decarboxylation*

Batch experiments were conducted using bushing-type ACE pressure tubes. In a typical experiment, 0.035 g of levulinic acid (3 mmol) was dissolved in 15 mL of a $K_2HPO_4/KH_2PO_4$ buffer solution (0.1/0.1 M in Milli-Q water, pH 6.9), followed by the addition of silver salt (3 mmol) and potassium persulfate (3 mmol). The reaction mixture was stirred and heated at 100 °C for 30 or 60 min.

The products in the liquid phase, including levulinic acid, acetic acid, and methyl ethyl ketone (MEK), were identified by GC-MS (Agilent 6980/5973, Les Ulis, France) using an Agilent J&W DB-5MS column (30 m × 0.25 mm, 0.25 µm). The injector and detector were maintained at 250 °C and 230 °C, respectively. The oven temperature was initially set to 70 °C and increased to 160 °C at a rate of 2 °C/min, followed by a further increase to 280 °C at 4 °C/min. A split ratio of 50 mL/min was used. The scan range was set from 25 to 300 m/z, and compound identification was performed using the NIST98.1 library. Levulinic acid, acetic acid, and MEK were also quantified by $^1$H NMR, with spectra recorded at 300 MHz in $D_2O$ using a Bruker Fourier 300 spectrometer (magnet system: 300 MHz/54 mm).

### *3.2. XPS Analyses*

XPS measurements were conducted using a Thermo Scientific K-alpha instrument (Waltham, MA, USA). Photoelectron emission spectra were recorded using Al-Kα radiation (hν = 1486.6 eV) from a monochromatized source, with an X-ray spot size of 400 µm. The

pass energy was set to 40 eV for high-resolution scans (and 150 eV for survey scans). A flood gun was employed to mitigate charging effects. The spectrometer was calibrated using the Au $4f_7/_2$ (83.9 ± 0.1 eV) and Cu $2p_3/_2$ (932.8 ± 0.1 eV) reference lines. XPS spectra were recorded in direct N(Ec) mode, with background subtraction performed using the Shirley method. Atomic concentrations were determined with an accuracy of ±10% using Scofield's atomic sensitivity factors, accounting for the transmission function of the analyzer, which was calibrated at different pass energies using Ag 3d and Ag MNN peaks from a reference silver sample. The binding energy scale was referenced to the C 1s peak of adventitious carbon (284.7 ± 0.1 eV), and photoelectron peaks were fitted using Lorentzian/Gaussian (L/G = 30) peak fitting.

### *3.3. XRD Analyses*

X-ray diffraction (XRD) patterns were obtained using a Bruker D8 Advance diffractometer equipped with a LynXeye 1D detector. The X-ray tube had a copper anode and operated without a monochromator. The primary wavelengths utilized were Kα (0.154059 nm) and Kα2 (0.15444 nm) radiation.

### *3.4. Thermodynamic Calculations*

Vapor–liquid and liquid–liquid equilibrium data were evaluated using the nonrandom two-liquid (NRTL) model, implemented through Simulis Thermodynamics, a thermodynamic properties and phase equilibria calculator provided by ProSim® software (https://www.prosim.net/wp-content/uploads/2019/12/Brochure-EN-Simulis-Thermodynamics_compressed.pdf, accessed on 3 October 2024) [70].

## 4. Conclusions

The decarboxylation of levulinic acid (LA) to produce methyl ethyl ketone (MEK) using the $AgNO_3/K_2S_2O_8$ system was systematically studied. MEK production was observed even in the absence of $AgNO_3$, but the presence of $K_2S_2O_8$ was essential for the reaction, even when Ag(II) species were involved. These results confirm that sulfate radicals ($SO_4\bullet-$) are directly responsible for LA decarboxylation, supporting a radical-based mechanism for MEK synthesis.

XRD and XPS analyses of the solid phases and surfaces throughout the reaction revealed that Ag(I) species were predominant, with minor traces of Ag(II) (as AgO) and elemental Ag(0), without any apparent reaction limitation. Acidification of the reaction medium was found to inhibit LA decarboxylation. By adjusting the pH to 5 and adding one more equivalent of $K_2S_2O_8$ after 30 min of reaction, a high LA conversion (up to 99%) and MEK yield of 87% were achieved in a second reaction cycle. Furthermore, $AgNO_3$ recycling was demonstrated to be feasible, making this process a promising step toward continuous MEK production, with $K_2S_2O_8$ being the only required reagent for replenishment.

**Author Contributions:** Conceptualization, E.V. and S.T.-R.; methodology, N.I.G.B., J.P., J.E., and P.B.; software, J.A.; formal analysis, N.I.G.B., J.E., and J.P.; data curation, N.I.G.B., J.P., J.E., and P.B.; writing—original draft preparation, N.I.G.B. and J.P.; writing—review and editing, P.B., C.V.-G., E.V., and S.T.-R.; project administration, S.T.-R. and C.V.-G.; funding acquisition, C.V.-G. and S.T.-R. All authors have read and agreed to the published version of the manuscript.

**Funding:** This work was supported by the European Union Seventh Framework Program for Research, Technological Development, and Demonstration (FP7/2007-2013) [Grant Agreement no. 605215].

**Institutional Review Board Statement:** Not applicable.

**Informed Consent Statement:** Not applicable.

**Data Availability Statement:** Data can be found in the Ph.D. thesis cited below.

**Acknowledgments:** This article is based on Ph.D. thesis results of Nydia I. Guzmán Barrera ("Eco-compatible synthesis of bio-based solvents for the paint and coating industry", 2018, Toulouse INP).

Guzmán Barrera acknowledges CONACyT (Mexico) for providing funding through Ph.D. scholarship no. 383910.

**Conflicts of Interest:** The authors declare no conflicts of interest.

## References


1. Sunnyside Corp. Available online: https://www.sunnysidecorp.com/product.php?p=t&b=s&n=847G1 (accessed on 3 October 2024).
2. Indestructible Paint. Available online: https://indestructible.co.uk/wp-content/uploads/download-manager-files/MEK.pdf (accessed on 3 October 2024).
3. Werpy, T.; Petersen, G.; Aden, A.; Bozell, J.; Holladay, J.; White, J.; Manheim, A.; Elliot, D.; Lasure, L.; Jones, S.; et al. Volumen I: Results of Screening for Potential Candidates from Sugars and Synthesis Gas. In *Top Value Added Chemicals from Biomass*; U.S. Department of Energy: Oak Ridge, TN, USA, 2004; p. 76.
4. Grand View Research. Available online: https://www.grandviewresearch.com/press-release/global-levulinic-acid-market (accessed on 3 October 2017).
5. Bozell, J.J.; Moens, L.; Elliott, D.C.; Wang, Y.; Neuenscwander, G.G.; Fitzpatrick, S.W.; Bilski, R.J.; Jarnefeld, J.L. Production of Levulinic Acid and Use as a Platform Chemical for Derived Products. *Resour. Conserv. Recycl.* **2000**, *28*, 227–239. [CrossRef]
6. Stapley, J.A.; Bemiller, J.N. The Hofer-Moest Decarboxylation of D-Glucuronic Acid and D-Glucuronosides. *Carbohydr. Res.* **2007**, *342*, 610–613. [CrossRef] [PubMed]
7. Mundle, S.O.C.; Kluger, R. Decarboxylation via Addition of Water to a Carboxyl Group: Acid Catalysis of Pyrrole-2-Carboxylic Acid. *J. Am. Chem. Soc.* **2009**, *131*, 11674–11675. [CrossRef]
8. Rodríguez, N.; Goossen, L.J. Decarboxylative Coupling Reactions: A Modern Strategy for C-C-Bond Formation. *Chem. Soc. Rev.* **2011**, *40*, 5030–5048. [CrossRef]
9. Mirkhani, V.; Tangestaninejad, S.; Moghadam, M.; Moghbel, M. Rapid and Efficient Oxidative Decarboxylation of Carboxylic Acids with Sodium Periodate Catalyzed by Manganese (III) Schiff Base Complexes. *Bioorg. Med. Chem.* **2004**, *12*, 903–906. [CrossRef] [PubMed]
10. Wang, D.; Hakim, S.H.; Alonso, D.M.; Dumesic, J.A. A Highly Selective Route to Linear Alpha Olefins from Biomass-Derived Lactones and Unsaturated Acids. *Chem. Commun.* **2013**, *49*, 7040–7042. [CrossRef]
11. Monig, J.; Chapman, R.; Asmus, K.-D. Effect of the Protonation State of the Amino Group on the *OH Radical Induced Decarboxylation of Amino Acids in Aqueous Solution. *J. Phys. Chem* **1985**, *89*, 3139–3144. [CrossRef]
12. Steffen, L.K.; Glass, R.S.; Sabahi, M.; Wilson, G.S.; Schoeneich, C.; Mahling, S.; Asmus, K.D. Hydroxyl Radical Induced Decarboxylation of Amino Acids. Decarboxylation vs. Bond Formation in Radical Intermediates. *J. Am. Chem. Soc.* **1991**, *113*, 2141–2145. [CrossRef]
13. Goldstein, S.; Czapski, G.; Cohen, H.; Meyerstein, D. Hydroxyl Radical Induced Decarboxylation and Deamination of 2-Methylalanine Catalyzed by Copper Ions. *Inorg. Chem.* **1992**, *31*, 2439–2444. [CrossRef]
14. Bobrowski, K.; Pogocki, D.; Schoneich, C. Mechanism of the Hydroxyl Radical-Induced Decarboxylation of 2-(Alkylthio)Ethanoic Acid Derivatives. *J. Phys. Chem.* **1993**, *97*, 13677–13684. [CrossRef]
15. Guitton, J.; Tinardon, F.; Lamrini, R.; Lacan, P.; Desage, M.; Francina, A. Decarboxylation of [1-$^{13}$C]Leucine by Hydroxyl Radicals. *Free Radic. Biol. Med.* **1998**, *25*, 340–345. [CrossRef] [PubMed]
16. Zhu, Y.; Li, X.; Wang, X.; Huang, X.; Shen, T.; Zhang, Y.; Sun, X.; Zou, M.; Song, S.; Jiao, N. Silver-Catalyzed Decarboxylative Azidation of Aliphatic Carboxylic Acids. *Org. Lett.* **2015**, *17*, 4702–4705. [CrossRef] [PubMed]
17. Fristad, W.E.; Fry, M.A.; Klang, J.A. Persulfate/Silver Ion Decarboxylation of Carboxylic Acids. Preparation of Alkanes, Alkenes, and Alcohols. *J. Org. Chem.* **1983**, *48*, 3575–3577. [CrossRef]
18. Wan, W.; Li, J.; Ma, G.; Chen, Y.; Jiang, H.; Deng, H.; Hao, J. Ag(I)-Catalyzed Oxidative Decarboxylation of Difluoroacetates with Activated Alkenes to Form Difluorooxindoles. *Org. Biomol. Chem.* **2017**, *15*, 5308. [CrossRef] [PubMed]
19. Wei, Y.; Hu, P.; Zhang, M.; Su, W. Metal-Catalyzed Decarboxylative C−H Functionalization. *Chem. Rev.* **2017**, *117*, 8864–8907. [CrossRef]
20. Kiméné, A.; Wojcieszak, R.; Paul, S.; Dumeignil, F. Catalytic Decarboxylation of Fatty Acids to Hydrocarbons over Non-Noble Metal Catalysts: The State of the Art. *J. Chem. Technol. Biotechnol.* **2018**, *94*, 658–669. [CrossRef]
21. Chumaidi, A.; Dewajani, H.; Sulaiman, M.A.; Angestine, F.; Putri, A.; Pravitasari, S.A. Effect of Temperature and Mg-Zn Catalyst Ratio on Decarboxylation Reaction to Produce Green Diesel from Kapok Oil with Saponification Pretreatment Using NaOH. *IOP Conf. Ser. Mater. Sci. Eng.* **2021**, *1073*, 012002. [CrossRef]
22. Chum, H.L.; Ratcliff, M.; Posey, F.L.; Turner, J.A.; Nozik, A.J. Photoelectrochemistry of Levulinic Acid on Undoped Platinized N-Titanium Dioxide Powders. *J. Phys. Chem.* **1983**, *87*, 3089–3093. [CrossRef]
23. Gong, Y.; Lin, L.; Shi, J.; Liu, S. Oxidative Decarboxylation of Levulinic Acid by Cupric Oxides. *Molecules* **2010**, *15*, 7946–7960. [CrossRef]
24. Gong, Y.; Lin, L. Oxidative Decarboxylation of Levulinic Acid by Silver(I)/Persulfate. *Molecules* **2011**, *16*, 2714–2725. [CrossRef]
25. Mehrer, C.R.; Rand, J.M.; Incha, M.R.; Cook, T.B.; Demir, B.; Hussain Motagamwala, A.; Kim, D.; Dumesic, J.A.; Pfleger, B.F. Growth-Coupled Bioconversion of Levulinic Acid to Butanone. *Metab. Eng.* **2019**, *55*, 92–101. [CrossRef] [PubMed]

26. Grilc, M.; Likozar, B. Levulinic Acid Hydrodeoxygenation, Decarboxylation and Oligmerization over NiMo/$Al_2O_3$ Catalyst to Bio-Based Value-Added Chemicals: Modelling of Mass Transfer, Thermodynamics and Micro-Kinetics. *Chem. Eng. J.* **2017**, *330*, 383–397. [CrossRef]
27. Novodárszki, G.; Valyon, J.; Illés, Á.; Dóbé, S.; Deka, D.; Hancsók, J.; Mihályi, M.R.; Hu, M.M.M. Heterogeneous Hydroconversion of Levulinic Acid over Silica-Supported Ni Catalyst. *React. Kinet. Mech. Catal.* **2019**, *126*, 795–810. [CrossRef]
28. Walling, C.; Camaioni, D.M. Role of Silver(II) in Silver-Catalyzed Oxidations by Peroxydisulfate. *J. Org. Chem.* **1978**, *43*, 3266–3271. [CrossRef]
29. Fristad, W.E.; Klang, J.A. Silver(I)/Persulfate Oxidative Decarboxylation of Carboxylic Acids. Arylacetic Acid Dimerization. *Tetrahedron Lett.* **1983**, *24*, 2219–2222. [CrossRef]
30. Tanner, D.D.; Osman, S.A.A. Oxidative Decarboxylation. On the Mechanism of the Potassium Persulfate-Promoted Decarboxylation Reaction. *J. Org. Chem.* **1987**, *52*, 4689–4693. [CrossRef]
31. Seiple, I.B.; Su, S.; Rodriguez, R.A.; Gianatassio, R.; Fujiwara, Y.; Sobel, A.L.; Baran, P.S. Direct C−H Arylation of Electron-Deficient Heterocycles with Arylboronic Acids. *J. Am. Chem. Soc.* **2010**, *132*, 13194–13196. [CrossRef]
32. Patel, N.R.; Flowers, R.A. Uncovering the Mechanism of the Ag(I)/Persulfate-Catalyzed Cross-Coupling Reaction of Arylboronic Acids and Heteroarenes. *J. Am. Chem. Soc.* **2013**, *135*, 4672–4675. [CrossRef]
33. Kan, J.; Huang, S.; Lin, J.; Zhang, M.; Su, W. Silver-Catalyzed Arylation of (Hetero)Arenes by Oxidative Decarboxylation of Aromatic Carboxylic Acids. *Angew. Chem. Int. Ed. Engl.* **2015**, *54*, 2199–2203. [CrossRef]
34. Chang, S.; Jian, A.; Wang, F.; Dong, L.L.; Wang, D.; Feng, B.; Shi, Y.T. Ag(I)/Persulfate-Catalyzed Decarboxylative Coupling of a-Oxocarboxylates with Organotrifluoroborates in Water under Room Temperature. *RSC Adv.* **2017**, *7*, 51928–51934. [CrossRef]
35. Anderson, J.M.; Kochi, J.K. Silver(I)-Catalyzed Oxidative Decarboxylation of Acids by Peroxydisulfate. Role of Silver(II). *J. Am. Chem. Soc.* **1970**, *92*, 1651–1659. [CrossRef]
36. Bartlett, P.D.; Cotman, J.D. The Kinetics of the Decomposition of Potassium Persulfate in Aqueous Solutions of Methanol. *J. Am. Chem. Soc.* **1949**, *71*, 1419–1422. [CrossRef]
37. Kolthoff, I.M.; Miller, I.K. The Chemistry of Persulfate. I. The Kinetics and Mechanism of the Decomposition of the Persulfate Ion in Aqueous Medium 1. *J. Am. Chem. Soc.* **1951**, *73*, 3055–3059. [CrossRef]
38. Berlin, A.A. Kinetics of Radical-Chain Decomposition of Persulfate in Aqueous Solutions of Organic Compounds. *Kinet. Catal.* **1986**, *27*, 34–39.
39. Berlin, A.A.; Kislenko, V.N.; Medvedevskikh, Y.G. Conditions for Occurrence of Long-Chain Oxidation Reaction of Organic Compounds by Persulfate in an Aqueous Medium. *Theor. Exp. Chem.* **1990**, *26*, 337–341. [CrossRef]
40. Hussain, I.; Zhang, Y.; Huang, S.; Du, X. Degradation of P-Chloroaniline by Persulfate Activated with Zero-Valent Iron. *Chem. Eng. J.* **2012**, *203*, 269–276. [CrossRef]
41. Couttenye, R.A.; Huang, K.C.; Hoag, G.E.; Suib, S.L. Evidence of Sulfate Free Radical ($SO4^-$) Formation under Heat-Assisted Persulfate Oxidation of MTBE. In Proceedings of the 19th Petroleum Hydrocarbons and Organic Chemicals in Ground Water: Prevention, Assessment, and Remediation, Conference and Exposition, Atlanta, GA, USA; 2002; pp. 345–350.
42. Dawes, G.J.S.; Scott, E.L.; Le Nôtre, J.; Sanders, J.P.M.; Bitter, J.H. Deoxygenation of Biobased Molecules by Decarboxylation and Decarbonylation—A Review on the Role of Heterogeneous, Homogeneous and Bio-Catalysis. *Green Chem.* **2015**, *17*, 3231–3250. [CrossRef]
43. Herrera-Ordonez, J. The Role of Sulfate Radicals and PH in the Decomposition of Persulfate in Aqueous Medium: A Step towards Prediction. *Chem. Eng. J. Adv.* **2022**, *11*, 100331–100341. [CrossRef]
44. Kimura, M.; Kawajiri, T.; Tanida, M. Kinetics of the Silver(I)-Catalyzed Decomposition of Peroxodisulphate in Aqueous Solution. *J. Chem. Soc. Dalton Trans.* **1980**, *5*, 726. [CrossRef]
45. Xia, X.-F.; Zhu, S.-L.; Chen, C.; Wang, H.; Liang, Y.-M. Silver-Catalyzed Decarboxylative Addition/Cyclization of Activated Alkenes with Aliphatic Carboxylic Acids. *J. Org. Chem.* **2016**, *81*, 1277–1284. [CrossRef]
46. Liu, J.; Fan, C.; Yin, H.; Qin, C.; Zhang, G.; Zhang, X.; Yi, H.; Lei, A. Synthesis of 6-Acyl Phenanthridines by Oxidative Radical Decarboxylation-Cyclization of α-Oxocarboxylates and Isocyanides. *Chem. Commun.* **2014**, *50*, 2145–2147. [CrossRef]
47. Hobbs, C.C.; Van't Hof, H. Liquid Phase Oxidation of Methyl Ethyl Ketone to Form Acetic Acid Therefrom. U.S. Patent No. US3947497A, 4 January 1974.
48. Clark, L.W. The Decarboxylation of Methylmalonic Acid Andn-Octadecylmalonic Acid in Normal Alkanols. *Int. J. Chem. Kinet.* **1976**, *8*, 609–624. [CrossRef]
49. Stockbridge, R.B.; Lewis, C.A.; Yuan, Y.; Wolfenden, R.; Wolfenden, R. Impact of Temperature on the Time Required for the Establishment of Primordial Biochemistry, and for the Evolution of Enzymes. *Proc. Natl. Acad. Sci. USA* **2010**, *107*, 22102–22105. [CrossRef]
50. Wolfenden, R.; Lewis, C.A.; Yuan, Y.; Yuan, Y. Kinetic Challenges Facing Oxalate, Malonate, Acetoacetate, and Oxaloacetate Decarboxylases. *J. Am. Chem. Soc.* **2011**, *133*, 5683–5685. [CrossRef]
51. Ng, H.N.; Calvo, C.; Faggiani, R.; IUCr. A New Investigation of the Structure of Silver Orthophosphate. *Acta Crystallogr. Sect. B Struct. Crystallogr. Cryst. Chem.* **1978**, *34*, 898–899. [CrossRef]
52. Keen, R.C. The Crystal Structure of Potassium Persulfate $K_2S_2O_8$. *Z. Krist.—Cryst. Mater.* **1935**, *91*, 129–135. [CrossRef]
53. Morris, M.; McMurdie, H.; Evans, E.; Paretzkin, B.; Groot, J.; Hubbard, C.; Carmel, S. *Standard X-ray Diffraction Powder Patterns*; National Bureau of Standards Monograph 25; U.S. Department of Commerce: Washington, DC, USA, 1976; p. 37.

54. Tibballs, J.E.; Nelmes, R.J.; McIntyre, G.J. The Crystal Structure of Tetragonal $KH_2PO_4$ and $KD_2PO_4$ as a Function of Temperature and Pressure. *J. Phys. C Solid State Phys.* **1982**, *15*, 37–58. [CrossRef]
55. Morgan, J.L.R.; Crist, R.H. The Photochemical Decomposition of Potassium Persulfate. I. *J. Am. Chem. Soc.* **1927**, *49*, 16–25. [CrossRef]
56. Morgan, J.L.R.; Crist, R.H. The Photochemical Decomposition of Potassium Persulfate. II. *J. Am. Chem. Soc.* **1927**, *49*, 338–346. [CrossRef]
57. Heidt, L.J. The Photolysis of Persulfate. *J. Chem. Phys.* **1942**, *10*, 297–302. [CrossRef]
58. House, D.A. Kinetics and Mechanism of Oxidations by Peroxydisulfate. *Chem. Rev.* **1962**, *62*, 185–203. [CrossRef]
59. Jette, E.R.; Foote, F. Precision Determination of Lattice Constants. *J. Chem. Phys.* **1935**, *3*, 605–616. [CrossRef]
60. Deb, A.; Manna, S.; Modak, A.; Patra, T.; Maity, S.; Maiti, D. Oxidative Trifluoromethylation of Unactivated Olefins: An Efficient and Practical Synthesis of α-Trifluoromethyl-Substituted Ketones. *Angew. Chem. Int. Ed.* **2013**, *52*, 9747–9750. [CrossRef]
61. Hatamura, M.; Yamaguchi, S.; Takane, S.; Chen, Y.; Suganuma, K. Decarboxylation and Simultaneous Reduction of Silver(I) β-Ketocarboxylates with Three Types of Coordinations. *Dalton Trans.* **2015**, *44*, 8993–9003. [CrossRef]
62. Standke, B.; Jansen, M. $Ag_3O_4$, the First Silver(II,III) Oxide. *Angew. Chem. Int. Ed. Engl.* **1986**, *25*, 77–78. [CrossRef]
63. Waterhouse, G.I.N.; Metson, J.B.; Bowmaker, G.A. Synthesis, Vibrational Spectra and Thermal Stability of $Ag_3O_4$ and Related $Ag_7O_8X$ Salts (X=$NO_3^-$,$ClO_4^-$,$HSO_4^-$). *Polyhedron* **2007**, *26*, 3310–3322. [CrossRef]
64. Kaspar, T.C.; Droubay, T.; Chambers, S.A.; Bagus, P.S. Spectroscopic Evidence for Ag(III) in Highly Oxidized Silver Films by X-Ray Photoelectron Spectroscopy. *J. Phys. Chem. C* **2010**, *114*, 21562–21571. [CrossRef]
65. Wang, W.; Cheng, B.; Yu, J.; Liu, G.; Fan, W. Visible-Light Photocatalytic Activity and Deactivation Mechanism of Ag3PO4 Spherical Particles. *Chem.—Asian J.* **2012**, *7*, 1902–1908. [CrossRef]
66. Turner, N.H.; Murday, J.S.; Ramaker, D.E. Quantitative Determination of Surface Composition of Sulfur Bearing Anion Mixtures by Auger Electron Spectroscopy. *Anal. Chem.* **1980**, *52*, 84–92. [CrossRef]
67. Gaarenstroom, S.W.; Winograd, N. Initial and Final State Effects in the ESCA Spectra of Cadmium and Silver Oxides. *J. Chem. Phys.* **1977**, *67*, 3500–3506. [CrossRef]
68. Tjeng, L.H.; Meinders, B.J.; Van Elp, J.; Ghinjsen, J.; Sawatzky, G.A.; Johnson, R.L. Electronic Structure of $Ag_2O$. *Phys. Rev. B* **1990**, *41*, 3190–3199. [CrossRef] [PubMed]
69. Kaushik, V.K. XPS Core Level Spectra and Auger Parameters for Some Silver Compounds. *J. Electron. Spectrosc. Relat. Phenom.* **1991**, *56*, 273–277. [CrossRef]
70. Simulis Thermodynamics, a Thermodynamic Properties and Phase Equilibria Calculator from ProSim® Software. Available online: https://www.prosim.net/en/product/simulis-thermodynamics-mixture-properties-and-fluid-phase-equilibria-calculations/ (accessed on 24 September 2024).